Charge dynamics of Co-doped $BaFe_2As_2$

2010 New J. Phys. 12 073036

(http://iopscience.iop.org/1367-2630/12/7/073036)

New Journal of Physics
The open-access journal for physics

Charge dynamics of Co-doped $BaFe_2As_2$

A Lucarelli[1], A Dusza[1], F Pfuner[1], P Lerch[2], J G Analytis[3,4], J-H Chu[3,4], I R Fisher[3,4] and L Degiorgi[1,5]

[1] Laboratorium für Festkörperphysik, ETH Zürich, CH-8093 Zürich, Switzerland
[2] Swiss Light Source, Paul Scherrer Institute, CH-5232 Villigen-PSI, Switzerland
[3] Geballe Laboratory for Advanced Materials and Department of Applied Physics, Stanford University, Stanford, CA 94305-4045, USA
[4] Stanford Institute for Materials and Energy Sciences, SLAC National Accelerator Laboratory, 2575 Sand Hill Road, Menlo Park, CA 94025, USA
E-mail: degiorgi@solid.phys.ethz.ch

New Journal of Physics **12** (2010) 073036 (13pp)
Received 23 April 2010
Published 27 July 2010
Online at http://www.njp.org/
doi:10.1088/1367-2630/12/7/073036

Abstract. We report on a thorough optical investigation over a broad spectral range and as a function of temperature of the charge dynamics in $Ba(Co_xFe_{1-x})_2As_2$ compounds for Co-doping ranging between 0 and 18%. For the parent compound as well as for $x = 0.025$, we observe the opening of a pseudogap, due to the spin-density-wave phase transition and inducing a reshuffling of spectral weight from low to high frequencies. For compounds with $0.051 \leqslant x \leqslant 0.11$, we detect the superconducting gap, while at $x = 0.18$ the material stays metallic at all temperatures. We describe the effective metallic contribution to the optical conductivity with two Drude terms, representing the combination of a coherent and an incoherent component, and extract the respective scattering rates. We establish that the dc transport properties in the normal phase are dominated by the coherent Drude term for $0 \leqslant x \leqslant 0.051$ and by the incoherent one for $0.061 \leqslant x \leqslant 0.18$, respectively. Finally, through spectral weight arguments, we give clear-cut evidence of moderate electronic correlations for $0 \leqslant x \leqslant 0.061$, which then cross over to values appropriate for a regime of weak interacting and nearly-free electron metals for $x \geqslant 0.11$.

[5] Author to whom any correspondence should be addressed.

Contents

1. Introduction

The discovery of superconductivity in several families of closely related iron-pnictides [1]–[4] has generated considerable interest, primarily because superconductivity is possible at high temperature in materials without CuO_2 planes, and has also induced a frenetic search for possible common mechanisms between them and the superconducting cuprates. Furthermore, these materials provide an interesting arena in which to study the impact of electronic correlations with respect to the emergence of structural/magnetic and superconducting phase transitions. One major difference between the phase diagrams of the copper-oxide and iron-pnictide superconductors is that the correlated metallic state in the cuprates derives from chemical doping of parent compounds in the strongly correlated Mott insulating state, while the parent compounds of the iron-pnictides are magnetically ordered bad metals. This means that magnetic ordering only partially gaps the Fermi surface (FS), inducing a spin-density-wave (SDW) broken-symmetry ground state without initiating an insulating one. The SDW transition can be suppressed by a variety of means, revealing in several cases a superconducting ground state [1]–[4].

A recent optical study of LaFePO [5] gave evidence of electronic correlations in the iron-pnictides, indicating that the kinetic energy of the electrons is reduced to half of that predicted by band theory of nearly free electrons, and implying that these systems could be on the verge of a Mott (insulator) transition. It may then be argued that transport in the iron-pnictides lies between the band-like itinerant and the Mott-like local magnetic moment extremes [5], and that both coherent and incoherent excitations must be present. An optical investigation of several iron-pnictides (AFe_2As_2, $A =$ Ba, Sr, Ca, Eu and Ni) further suggests the presence of two subsystems: a coherent Fermi liquid one, out of which superconductivity evolves and a temperature-independent incoherent one, acting as background to the excitation spectrum but still affected by superconductivity [6]. Finally, x-ray absorption and resonant inelastic x-ray scattering reveal weak electronic correlations in the iron-pnictides [7].

Many-body effects, like electron–electron or electron–phonon interactions and even magnetic fluctuations, have a tremendous impact on the excitation spectrum, leading to characteristic fingerprints, like the opening of energy (correlation) gaps and potentially anomalous redistribution of spectral weight, so well documented in the cuprates ([8] and references therein). Optical methods are in principle an ideal spectroscopic tool for addressing these issues. Our strategy consists here of comparing the electrodynamic response of $Ba(Co_xFe_{1-x})_2As_2$ for several Co-dopings, which belong to the so-called 122 family and are prominent examples of oxygen-free iron-pnictide superconductors ([9] and references therein). We present systematic measurements across the phase diagram, from underdoped

non-superconducting ($x = 0$ and 0.025), to underdoped superconducting ($x = 0.051$), to near optimal doping ($x = 0.061$), to overdoped superconducting ($x = 0.11$) and finally to overdoped non-superconducting ($x = 0.18$) compositions. Particular emphasis is devoted to the impact of the various transitions on the charge dynamics in these Co-doped 122 materials. Our primary goal is to exploit their electrodynamic response in order to shed light on the scattering processes of the itinerant charge carriers as well as to establish with spectral weight argument their degree of electronic correlations.

2. Experiment and results

Single crystals of $Ba(Co_xFe_{1-x})_2As_2$ with $x = 0$, 2.5, 5.1, 6.1, 11 and 18% were grown from a self-flux using similar conditions to published methods [9, 10]. The crystals have a plate-like morphology, with the c-axis perpendicular to the plane of the plates, and grow up to several millimeters on a side. Our specimens were from the same growth batches used for the dc transport characterization [9]. For $x = 0$, the coincident structural (tetragonal-orthorhombic) and SDW transitions occur at $T_{TO} = T_{SDW} = 135$ K, whereas for $x = 0.025$ they develop at $T_{TO} = 98$ K and $T_{SDW} = 92$ K, respectively. The compound with $x = 0.051$ undergoes first a structural transition at $T_{TO} = 50$ K and then an SDW one at $T_{SDW} = 37$ K. In the latter compound, a superconducting state finally develops below $T_c = 19$ K. At optimal doping $x = 0.061$ as well as for $x = 0.11$, there is only the transition to the superconducting state at $T_c = 23$ and 14 K, respectively. The $x = 0.18$ compound does not undergo any phase transitions and is metallic at all temperatures [9].

We perform optical reflectivity measurements as a function of temperature from the far-infrared (FIR) to the ultraviolet (UV). This is the prerequisite in order to perform reliable Kramers–Kronig (KK) transformation from where we obtain the phase of the complex reflectance and then all optical functions, including the real part $\sigma_1(\omega)$ of the complex optical conductivity. To this end, we extended the $R(\omega)$ spectra with the Hagen–Rubens (HR) extrapolation for $\omega \to 0$ in the metallic phase [11, 12] and by setting $R(\omega)$ equal to total reflection below a characteristic frequency ω_g (see below) in the superconducting state. The σ_{dc} values used in the HR expression coincide with dc transport data collected from samples from the same batches [9]. At high frequencies the standard extrapolations $R(\omega) \sim \omega^{-s}$ with $2 \leqslant s \leqslant 4$ were employed [11, 12].

Figure 1 shows the optical reflectivity $R(\omega)$ for all investigated compounds below 5000 cm^{-1} at selected temperatures for the normal state as well as for the SDW or superconducting state. The inset emphasizes the high-frequency $R(\omega)$ spectrum up to the UV spectral range, which is representative of all dopings. For Co-dopings $x \leqslant 0.06$, $R(\omega)$ is reminiscent of an overdamped-like behavior, displaying a gentle increase in $R(\omega)$ at frequencies from UV to the mid-infrared (MIR) (figure 1, inset) and then a steeper one below about 500 cm^{-1}. For Co-dopings $x \geqslant 0.11$, a sharper plasma edge in $R(\omega)$ develops below about 2000 cm^{-1}, leading to larger $R(\omega)$ values than for $x \leqslant 0.061$. This is consistent with the enhancemnt of metallicity with increasing Co-doping, as evinced from the dc transport properties [9]. The temperature dependence extends over a large energy interval up to about 3000 cm^{-1}. This already anticipates an important reshuffling of spectral weight up to energies much larger than the energy scales defined by the phase transition critical temperatures. For $x = 0$ in the SDW state, we recognize the depletion of $R(\omega)$ in the infrared range and its low-frequency enhancement at low temperatures, consistent with previous data [13, 14]. Such a behavior turns out to be less pronounced for the $x = 0.025$ doping. For $x = 0.051$, 0.061

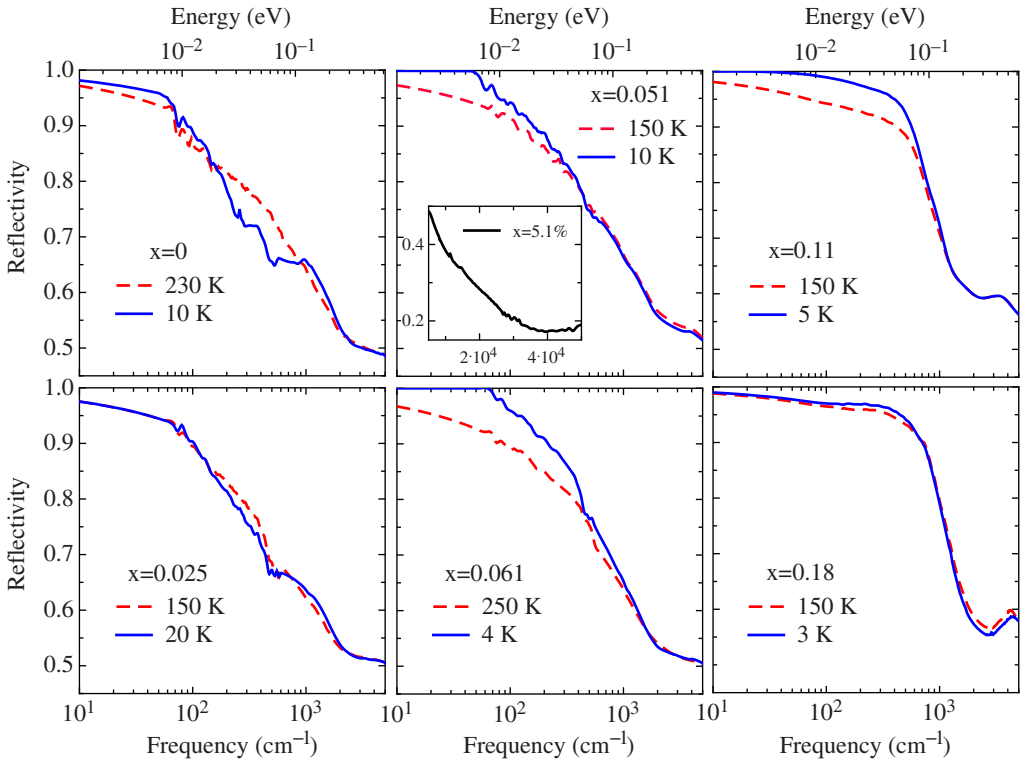

Figure 1. Optical reflectivity of $Ba(Co_xFe_{1-x})_2As_2$ for x ranging from 0 to 18% in the spectral range below 5000 cm^{-1} at selected temperatures above and below the various phase transitions. The inset displays $R(\omega)$ at 300 K for $x = 0.051$ up to the UV spectral range, which is representative of all compounds.

and 0.11, $R(\omega)$ progressively increases in FIR with decreasing temperature and approaches total reflection at the finite frequency ω_g in the superconducting state (i.e. $T \ll T_c$). $R(\omega)$ for $x = 0.18$ is metallic-like at all temperatures. Rather sharp and weak features at about 80 and 260 cm^{-1} are identified in $R(\omega)$ of the parent compound at low temperatures, which can be ascribed to the lattice vibrational modes [13], [15]–[17]. The enhanced metallicity of $R(\omega)$ for higher Co-dopings screens these modes. We do not observe any anomalies in the phonon features or the appearance of new modes when undergoing the structural phase transition[6].

Figure 2 highlights the temperature dependence of $\sigma_1(\omega)$ for all dopings in the energy ranges pertinent to the SDW and superconducting transition. The resulting $\sigma_1(\omega \to 0)$ limits at $T > T_{SDW}$ or T_c are in fair agreement with the dc results, thus confirming the consistency of the KK procedure. At low frequencies, the overall temperature dependence of $\sigma_1(\omega)$ for all compounds agrees, where appropriate, with previous data [13], [15]–[17]. In the parent ($x = 0$) and underdoped non-superconducting compound ($x = 0.025$), $\sigma_1(\omega)$ slightly decreases below 2000 cm^{-1} in the normal state, leading to a shallow minimum prior to the onset of the (narrow) Drude component in FIR. This is the consequence of the overdamped behavior of $R(\omega)$, which in our samples seems to be more pronounced than in previous work [13, 15]. This probably originates from the somehow smaller dc conductivity of our specimens [9] than in other samples. These deviations turn out, however, to be uninfluential for the data analysis and

[6] The phonon features in our spectra are too weak, so that possible mode splitting, due to the lowering of the crystal symmetry, as well as signature for mode softening is beyond our experimental resolution.

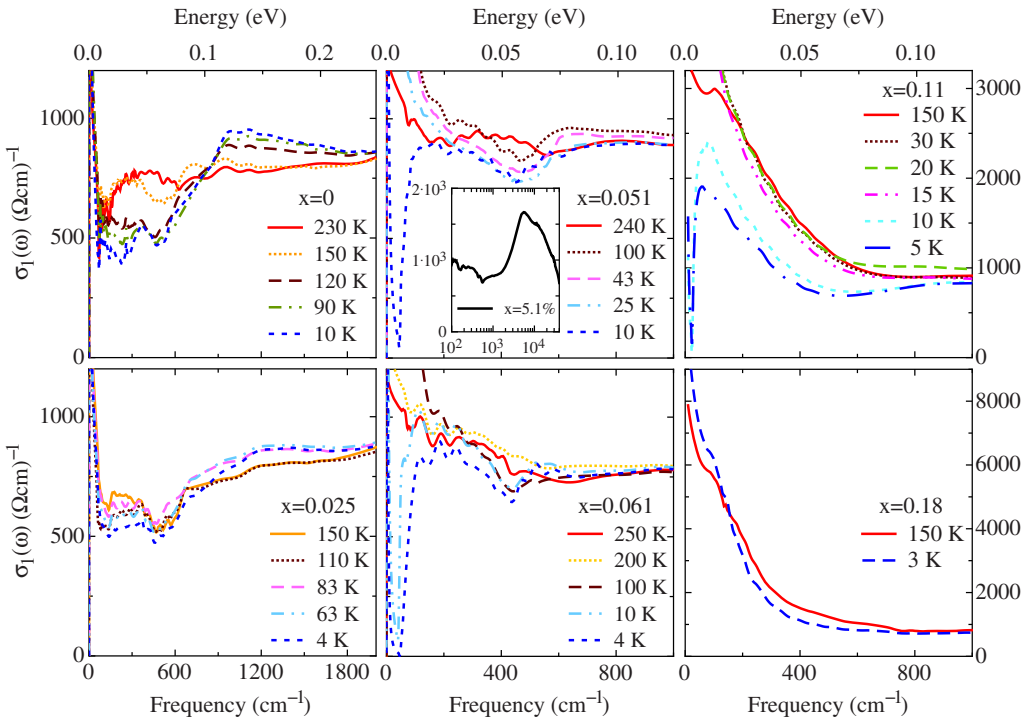

Figure 2. Real part $\sigma_1(\omega)$ of the optical conductivity for $Ba(Co_xFe_{1-x})_2As_2$ with x ranging from 0 to 18% in the FIR and MIR spectral range at selected temperatures above and below the various phase transitions. The inset displays $\sigma_1(\omega)$ at 300 K for $x = 0.051$, emphasizing its representative shape for all compounds at high frequencies up to the UV.

their overall interpretation. The excitation spectrum at high frequencies, shown in the inset of figure 2, is identical for all Co-dopings and is consistent with previous investigations [13, 16]. There is a strong absorption band peaked at about 5000 cm^{-1}, further characterized by a broad high-frequency tail and generally ascribed to the contribution due to the electronic interband transitions. $\sigma_1(\omega)$ for $x = 0$ suddenly decreases below 800 cm^{-1} at temperatures below T_{SDW}. This leads to a depletion in the range between 200 and 800 cm^{-1} (figure 2), inducing a removal of spectral weight. The depletion and the peak at about 800 cm^{-1} in $\sigma_1(\omega)$ are indicative of the opening of a pseudogap, which we identify with the SDW single particle excitation [13, 14]. For $x = 0.025$ Co-doping, the depletion and the (pseudo)gap feature in $\sigma_1(\omega)$ are less evident and pronounced, even though there is a spectral weight redistribution, leading again to its overshoot above 700 cm^{-1} for temperatures below T_{SDW}. The signatures for the SDW pseudogap-like excitation as well as the related spectral weight redistribution are no longer very distinct for the $x = 0.051$ Co-doping[7]. For the latter compound as well as at and above the optimal Co-doping

[7] An attentive look at the data reveals, nevertheless, an incipient depletion at 100 K, which becomes stronger at 43 K, a temperature between T_{TO} and T_{SDW}. The depletion at 43 K is accompanied by a reshuffling of the spectral weight at high frequencies, resulting in the formation of a barely observable pseudogap-like feature. By approaching the superconductivity phase transition, these weak features are totally washed out. The spectral weight redistribution involved at temperatures between 100 and 10 K in the energy interval between 200 and 1000 cm^{-1} is, moreover, too small to allow more robust considerations about the possible coexistence of the SDW and the superconducting state.

($x = 0.061$ and 0.11, respectively), the total reflection at $\omega \leqslant \omega_g$ for $T \ll T_c$ leads instead to the opening of the superconducting gap [6], [16]–[18]. The removed spectral weight is shifted into the collective excitation at zero frequency. While our data in the superconducting state overall agree with previous work, they do not extend low enough in frequencies, in order to allow an elaborated analysis in terms of multiple superconducting gaps [16, 17]. Finally, the electrodynamic response of the $x = 0.18$ compound merely displays a simple metallic behavior.

Overall, there are three energy intervals characterizing $\sigma_1(\omega)$ for all Co-dopings: the effective metallic contribution at low frequencies, the MIR band covering the energy range between 500 and 1500 cm^{-1} and the electronic interband transitions with onset at about 2000 cm^{-1} and peaked at 5000 cm^{-1}. The metallic part and the MIR band turn out to experience the strongest temperature dependence at T_c and/or T_{SDW} (figure 2), while the high frequency excitations (figure 2, inset) are temperature independent.

3. Discussion

Since the superconducting properties were intensively studied by different groups on selected members of the iron-pnictide families [6], [16]–[18], we will mainly address here the normal and SDW state properties. To this end, we apply the common and well-established phenomenological Drude–Lorentz approach [11, 12]. In order to account for the various bands crossing the Fermi level [19, 20], and consistent with previous investigations [6], we ascribe two Drude contributions (one narrow and one broad) to the effective metallic part of $\sigma_1(\omega)$ and a series of Lorentz harmonic oscillators (h.o.) for all excitations (phononic and electronic) at finite frequencies,

$$\tilde{\epsilon}(\omega) = \epsilon_1(\omega) + \mathrm{i}\epsilon_2(\omega) = \epsilon_\infty - \frac{\omega_{\mathrm{PN}}^2}{\omega^2 - \mathrm{i}\omega\Gamma_{\mathrm{N}}} - \frac{\omega_{\mathrm{PB}}^2}{\omega^2 - \mathrm{i}\omega\Gamma_{\mathrm{B}}} + \sum_j \frac{S_j^2}{\omega_j^2 - \omega^2 - \mathrm{i}\omega\gamma_j}, \tag{1}$$

where ϵ_∞ is the optical dielectric constant, $\omega_{\mathrm{PN/B}}$ and $\Gamma_{\mathrm{N/B}}$ are the plasma frequencies and the widths of the narrow and broad Drude peaks, whereas ω_j, γ_j and S_j^2 are the center-peak frequency, the width and the mode strength for the jth Lorentz h.o., respectively. $\sigma_1(\omega)$ is then obtained from $\sigma_1(\omega) = \omega\epsilon_2(\omega)/4\pi$. While the approach with two Drude terms implies the existence of two electronic subsystems, it is too phenomenological to allow speculations on whether the two Drude components have specific orbital character [21]. Consistent with the notion introduced in [6], the narrow Drude term is identified with the coherent part of the excitation spectrum, while the broad one acts as background to $\sigma_1(\omega)$ and represents its incoherent contribution[8]. Besides the sharp and weak h.o.s for the phonon modes, three broad ones for the strong absorption features leading to the peak at about 5000 cm^{-1} and one for the

[8] Within the generalized Drude approach [12], allowing us to extract the frequency dependence of the scattering rate $\Gamma(\omega)$, one can establish that $\Gamma(\omega) \leqslant \omega$ at infrared frequencies for $x \leqslant 0.051$. This signifies the presence of coherent quasiparticles. The opposite applies for x above the optimal doping, so that incoherent quasiparticles contribute to the dc transport [5]. This is also consistent with our findings on the relationship between the dc transport properties and the scattering rates of the narrow and broad Drude terms for Co content above and below the optimal doping, respectively (figure 3).

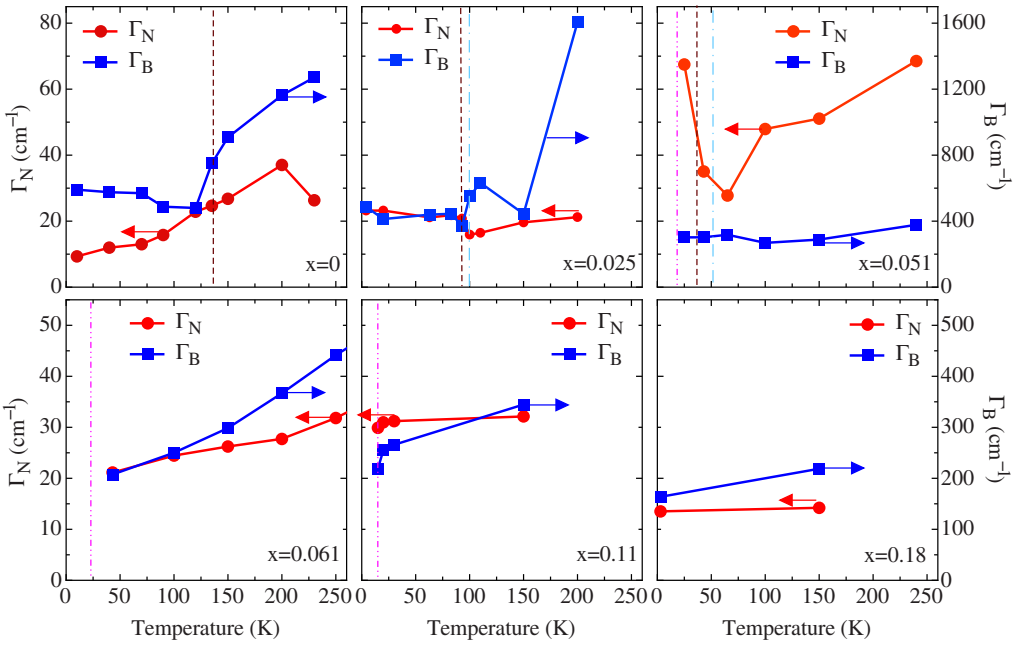

Figure 3. Temperature dependence of the scattering rate of the narrow (Γ_N) and broad (Γ_B) Drude terms (equation (1)), used to fit the effective metallic contribution to the optical conductivity of $Ba(Co_xFe_{1-x})_2As_2$ with x ranging from 0 to 18%. The thin dashed-dotted, dashed and dashed-dotted-dotted vertical lines mark, when appropriate, the structural (tetragonal-orthorhombic), SDW and superconducting transitions, respectively.

MIR band were also considered in our fits[9]. The inset of figure 6 depicts the Drude terms as well as the h.o. for the MIR band, which fully account for the temperature dependence of the spectra. We systematically apply this fit procedure for each Co-doping at all temperatures, obtaining everywhere a comparable good fit quality (e.g. the spectra at 120 K for $x = 0$, figure 6, inset).

First, we extract the scattering rates Γ_N and Γ_B of both narrow and broad Drude terms, respectively. Γ_N and Γ_B are shown in figure 3. At the phase transition temperatures for $0 \leqslant x \leqslant 0.051$, both scattering rates display anomalies, while for $0.061 \leqslant x \leqslant 0.18$ they monotonically decrease or stay constant with decreasing temperatures, consistent with a rather conventional metallic behavior. More compelling at this point is the comparison with the dc transport properties. Inspired by [6], we argue that the coherent contribution to the dc transport is given by

$$\rho_{dc}^{\text{coherent}} = (\rho_{dc}^{-1}(T) - \sigma_{dc}^{\text{broad Drude}})^{-1}, \tag{2}$$

where $\rho_{dc}(T)$ is the measured resistivity reported in [9] and $\sigma_{dc}^{\text{broad Drude}}$ is the $\omega \to 0$ limit of the broad Drude term. As shown in figure 4 (upper panels), we discover that Γ_N scales to

[9] For $x = 0$ and 0.025, two additional h.o.s, located in the high- and low-frequency tail of the narrow Drude and MIR band h.o., respectively, were employed in order to better reproduce the shape of $\sigma_1(\omega)$. These contributions were consistently included in the spectral weight analysis of the Drude terms and MIR band in relation to figures 5 and 6.

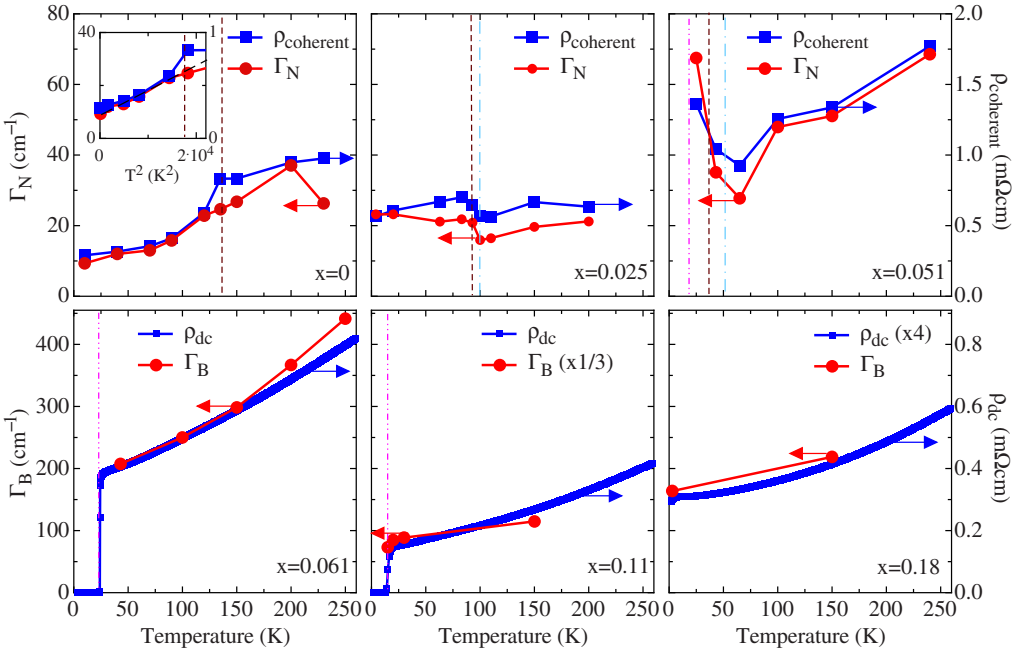

Figure 4. Upper panels: comparison between the scattering rate of the narrow Drude term (Γ_N) and the coherent contribution to the dc transport properties (equation (2)) for $Ba(Co_xFe_{1-x})_2As_2$ with x ranging from 0 to 5.1%. The inset for $x = 0$ emphasizes the T^2 dependence of both Γ_N and $\rho_{dc}^{coherent}$ at $T < T_{SDW}$. Lower panels: comparison between the scattering rate of the broad Drude term (Γ_B) and the dc transport properties ($\rho_{dc}(T)$; [9]) for $Ba(Co_xFe_{1-x})_2As_2$, with x ranging from 6.1 to 18%. The thin dashed-dotted, dashed and dashed-dotted-dotted vertical lines mark, when appropriate, the structural (tetragonal-orthorhombic), SDW and superconducting transitions, respectively.

the calculated quantity $\rho_{dc}^{coherent}(T)$ for Co-dopings $x \leqslant 0.051$.[10] Interestingly enough, Γ_N and $\rho_{dc}^{coherent}(T)$ for $x = 0$ follow a T^2 dependence at low temperatures (figure 4, inset), consistent with previous findings and uncovering a Fermi liquid behavior [6]. For Co-dopings $x \geqslant 0.061$, it turns out that Γ_B scales fairly well with the total resistivity $\rho_{dc}(T)$ [9], as shown in the lower panels of figure 4. This derives from the fact that the two Drude terms, globally describing the low frequency part of $\sigma_1(\omega)$, are no longer so distinct for $x \geqslant 0.061$ as for $x \leqslant 0.051$, and that the incoherent contribution largely dominates $\sigma_1(\omega)$ over the coherent one. Consequently, the decomposition of the metallic contribution in $\sigma_1(\omega)$ in two independent conduction channels is not unique anymore[11]. We thus suggest that for Co-dopings, where the FS may be gapped by

[10] By assuming that $\sigma_{dc}(T)$ can be expressed as the $\omega \to 0$ limit of $\sigma_1(\omega)$ for both narrow and broad Drude terms, and since $\sigma_1(\omega \to 0)$ well matches with the dc conductivity ([9]) at any temperatures for all dopings, one may achieve an equivalent good agreement between Γ_N and $\rho_{dc}^{coherent}$ by using values of the latter quantity directly extracted from the fits.

[11] One could alternatively argue that in this case *all* itinerant charge carriers equally feel two scattering channels with scattering rates Γ_N and Γ_B. Consequently, in the first approximation, one can define $\Gamma_{total} = \Gamma_N + \Gamma_B$ after Matthiessen's rule [22]. Since $\Gamma_N \ll \Gamma_B$, Γ_{total} would also nicely scale with $\rho_{dc}(T)$, further reinforcing our argument.

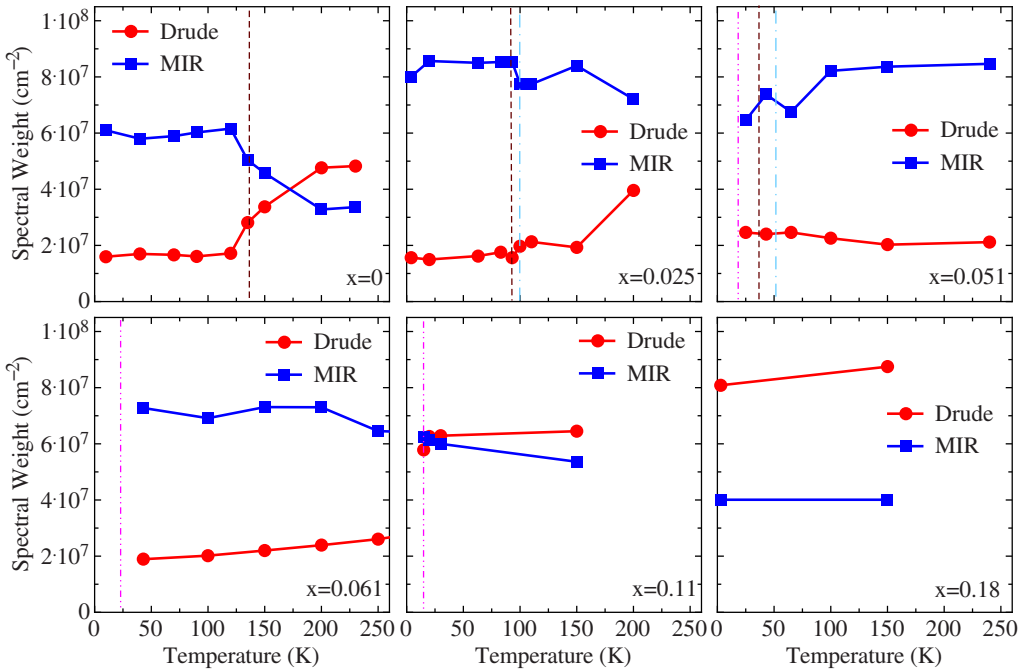

Figure 5. Temperature dependence of the integrated spectral weight (equation (3) and see footnote 11) of the Drude components and of the MIR band in $\sigma_1(\omega)$ (see the inset of figure 6) for $Ba(Co_xFe_{1-x})_2As_2$ with x ranging from 0 to 18%. The thin dashed-dotted, dashed and dashed-dotted-dotted vertical lines mark, when appropriate, the structural (tetragonal-orthorhombic), SDW and superconducting transitions, respectively.

the SDW instability, Γ_N shapes the coherent contribution to the dc transport properties, while for Co-dopings above $x = 0.061$ the scattering rate of the broad (incoherent) Drude term mainly determines the dc transport (see footnote 7).

Another relevant quantity, characterizing the electrodynamic response, is the integrated spectral weight encountered in $\sigma_1(\omega)$ up to a cut-off frequency ω', which is achieved through the well-known f-sum rule [11, 12],

$$SW(\omega') = \frac{120}{\pi} \int_0^{\omega'} \sigma_1(\omega)\, \mathrm{d}\omega. \tag{3}$$

It turns out that the sum rule as a function of temperature is almost fully satisfied for ω' between 2000 and 3000 cm^{-1} for all Co-dopings, irrespective of whether there is a phase transition into a SDW or a superconducting state. This is at variance to the high-temperature superconducting cuprates, where the spectral weight, merging into the collective state at $\omega = 0$ as a consequence of the opening of the superconducting gap along the c-axis orthogonal to the CuO_2 plane, is actually transferred from very high energy scales. This means equivalently that in the cuprates only 50% of the weight pertaining to the collective state is recovered at MIR energies [23].

In order to investigate how the spectral weight redistributes as a function of temperature among the various components in $\sigma_1(\omega)$, we can further exploit our phenomenological approach. Figure 5 summarizes indeed the temperature dependence of the spectral weight

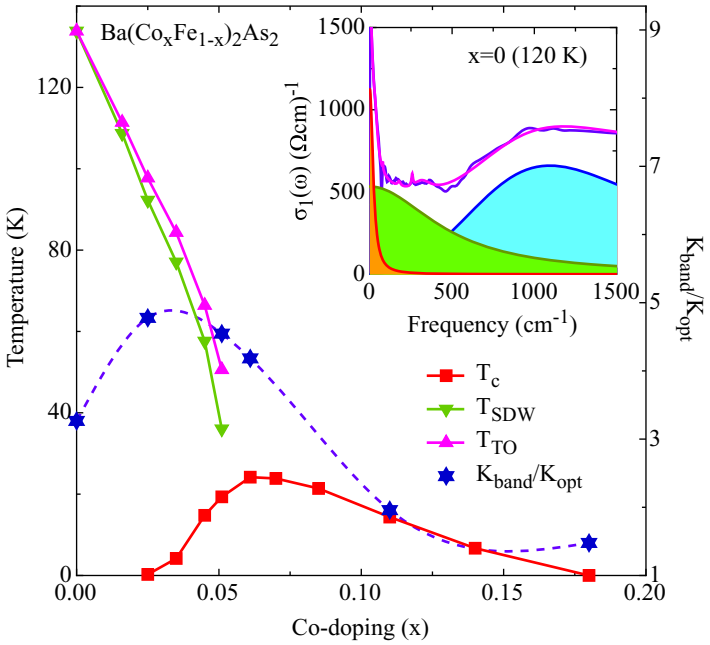

Figure 6. Phase diagram of $Ba(Co_xFe_{1-x})_2As_2$, reproduced from [9] (left y-axis), and the average of the ratio K_{band}/K_{opt} (equation (4)) calculated at low and high temperatures (right y-axis). All data interpolations are shown by spline lines as a guide to the eye. The inset displays the optical conductivity at 120 K for the parent compound ($x = 0$) with the total Drude–Lorentz fit and its low-frequency components, i.e. the narrow and broad Drude terms as well as the MIR h.o. (see text and equation (1)). The shaded areas emphasize the respective spectral weights ($\int \sigma_{1N}(\omega)d\omega$, $\int \sigma_{1B}(\omega)d\omega$ and $\int \sigma_1^{MIR}(\omega)d\omega$, equation (4)).

encountered in the Drude terms and in the MIR band (inset of figure 6)[12]. For the parent compound ($x = 0$) there is an obvious depletion of weight in the Drude part at T_{SDW}, which is reshuffled into the MIR band. At $x = 0.025$ there is a similar yet more modest redistribution of weight at T_{SDW}. At $x = 0.051$ the Drude part of $\sigma_1(\omega)$ slightly gains weight with decreasing temperature at the cost of the MIR part[13]. The disappearance of the SDW gap upon Co-doping could have various origins. A first possible scenario might rely on the role played by the doping-induced disorder, which progressively releases the favorable nesting conditions, so crucial for magnetic order, and thus favors the suppression of the SDW gap feature, as observed for $x = 0.025$ and 0.051. Neutron scattering experiments show, on the other hand, that the ordered moment also decreases with increasing Co-concentration, eventually supporting a local moment picture for the quenching of the SDW state [24]. An imbalance of electrons and holes could affect the nesting condition as well. This latter scenario, however, needs further investigation. We should also add that, for $x = 0.051$, T_c is pretty close to T_{SDW}. Therefore, by the time the temperature is low enough to allow a fully developed SDW (pseudo)gap, the system is already in the superconducting state and it is no surprise that almost no signatures of the SDW transition

[12] Equation (3) is equal to the sum of the square of the plasma frequencies for the Drude terms and to the mode strength of the h.o. for the MIR band (see footnote 8).

[13] With decreasing temperature, the h.o. for the MIR absorption feature in $x = 0.051$ tends to redistribute its spectral weight towards the low-frequency tail of the electronic interband transitions.

are optically detected for $x = 0.051$ (see footnote 6). For higher Co-dopings (i.e. $x \geqslant 0.061$), the spectral weights of the Drude and MIR components are almost temperature independent and interestingly enough the Drude weight increases with respect to the MIR one, the latter observation being an indication of the enhancement of metallicity with increasing Co-dopings.

We propose a scenario where the conduction band derives from d-states and splits into two parts: a purely itinerant one close to the Fermi level and represented by the two Drude components as well as by a bottom part with states below the mobility edge and thus rather localized. This latter part gives rise to the MIR band in $\sigma_1(\omega)$, which turns out to be strongly temperature dependent upon magnetic ordering and affected by the opening of the SDW gap. We can then consider the following ratio,

$$K_{\mathrm{opt}}/K_{\mathrm{band}} = \frac{\int \sigma_{1\mathrm{N}}(\omega)\mathrm{d}\omega + \int \sigma_{1\mathrm{B}}(\omega)\mathrm{d}\omega}{\int \sigma_{1\mathrm{N}}(\omega)\mathrm{d}\omega + \int \sigma_{1\mathrm{B}}(\omega)\mathrm{d}\omega + \int \sigma_1^{\mathrm{MIR}}(\omega)\mathrm{d}\omega}, \tag{4}$$

where $\sigma_{1\mathrm{N}}(\omega)$, $\sigma_{1\mathrm{B}}(\omega)$ and $\sigma_1^{\mathrm{MIR}}(\omega)$ are the components of the optical conductivity due to the narrow and broad Drude terms and to the MIR band within our phenomenological approach (equation (1) and inset of figure 6), respectively. Equation (4) represents the ratio between the spectral weight encountered in $\sigma_1(\omega)$ in the Drude components (K_{opt}) and the total spectral weight collected in $\sigma_1(\omega)$ up to the onset of the electronic interband transitions (i.e. Drude components together with the MIR absorption feature, K_{band}). By assuming the conservation of the total charge carriers density, equation (4) is, in principle, proportional to the ratio between the effective mass at low energy scales, which includes all renormalizations of local character or due to spin fluctuations, and the effective mass at high energies, which only includes local effects of Hubbard type [25]. Therefore, the reduction of K_{opt} with respect to K_{band} (equation (4)) would solely derive from the effective mass renormalization. Obviously in a multiband scenario, as it applies to the iron-pnictides, it could well be that the rearrangement of the total number of charge carriers between hole and electron bands is such that the total charge carrier density is not conserved. In this case, the spectral weight reduction in the effective metallic contribution of $\sigma_1(\omega)$ might not be due to the effective mass (i.e. correlation effects) alone [26]. One should then carefully address the effect of electron–electron interactions on both effective mass and charge carrier concentration. Such a debate is beyond the scope of the present discussion. Nevertheless, in the spirit of [5], we are confident that equation (4) is an alternative estimation, exclusively obtained from the experimental findings, of the ratio between the optical kinetic energy extracted from $\sigma_1(\omega)$ and the band kinetic energy extracted from the band structure within the tight-binding approach. We have calculated $K_{\mathrm{opt}}/K_{\mathrm{band}}$ after equation (4) at high and low temperatures, but still corresponding to the normal or SDW state[14]. Our $K_{\mathrm{opt}}/K_{\mathrm{band}}$ for

[14] It is worth noting that superconductivity in the iron-pnictides emerges in the close proximity of an antiferromagnetic (AF) ground state, thus implying the important role of AF fluctuations in the pairing mechanism of the itinerant charge carriers. As anticipated in [6], both Drude terms are affected by the superconducting transition (figure 2). It is consequently legitimate to consider the total spectral weight of both Drude terms (i.e. involving all ungapped charge carriers in the normal state) for the definition of the optical kinetic energy. For low Co-dopings (particularly for $x \leqslant 0.025$), the SDW instability and the resulting FS gapping at low temperatures within the SDW state obviously lead to a reshuffling of spectral weight in $\sigma_1(\omega)$ below 2000 cm^{-1}, thus affecting both quantities K_{opt} and K_{band} in equation (4). Therefore, $K_{\mathrm{band}}/K_{\mathrm{opt}}$ for the parent and underdoped non-superconducting compounds ($x \leqslant 0.025$) is larger at $T < T_{\mathrm{SDW}}$ than above. Nevertheless, it turns out that $K_{\mathrm{band}}/K_{\mathrm{opt}}$, both at high and low temperature, behaves similarly as a function of Co-doping, so that both estimations converge with increasing doping content and are basically identical for $x \geqslant 0.11$. Thus, the proposed average value in figure 6 suitably gives an overall trend for the degree of electronic correlations.

$x = 0$ is consistent with the value reported in figure 3 of [5] for the same compound, therefore reinforcing the validity of our spectral weight arguments. The inverse of $K_{\rm opt}/K_{\rm band}$, which then defines the degree of electronic correlations, is plotted in figure 6 as an average of the $K_{\rm band}/K_{\rm opt}$ values at low and high temperatures (see footnote 13) within the phase diagram of the Co-doped 122 iron-pnictides [9]. $K_{\rm band}/K_{\rm opt}$ thus tracks the evolution of the superconducting dome in the phase diagram of $Ba(Co_xFe_{1-x})_2As_2$. Interestingly enough, electronic correlations seem to be stronger for the parent compound and for Co-dopings $x \leqslant 0.061$ than for those in the overdoped range. There is indeed evidence of a crossover from a regime of moderate correlations for $x \leqslant 0.061$ to a nearly free and non-interacting electron gas system for $x \geqslant 0.11$.

4. Conclusions

We have provided a comprehensive optical investigation of $Ba(Co_xFe_{1-x})_2As_2$ with several Co-dopings, spanning the entire phase diagram. Besides establishing a direct relationship between the scattering rates and the dc transport properties, we have shed light on the spectral weight redistribution between the itinerant and the localized portion of the conduction band. We argue that the 122 iron-pnictides fall in the regime of moderate electronic correlations for the parent compound and close to optimal doping, while a conventional metallic behavior in the nearly free electron limit is recovered at the opposite, overdoped, end of the superconducting dome in their phase diagram.

Acknowledgments

We thank M Dressel, L Benfatto, D Basov, M Qazilbash, R Hackl and A Chubukov for fruitful discussions and P Butti for valuable help in collecting part of the data. This work was supported by the Swiss National Foundation for the Scientific Research within the NCCR MaNEP pool. This work was also supported by the Department of Energy, Office of Basic Energy Sciences, under contract number DE-AC02-76SF00515.

Note added. While preparing the manuscript for submission, we became aware of the work reported in [27], which presents similar data for part of the samples discussed here.

References

[1] Kamihara Y *et al* 2008 *J. Am. Chem. Soc.* **130** 3296
[2] Rotter M *et al* 2008 *Phys. Rev. Lett.* **101** 107006
[3] Chen X H *et al* 2008 *Nature* **453** 761
[4] Sefat A S *et al* 2008 *Phys. Rev. Lett.* **101** 117004
[5] Qazilbash M M *et al* 2009 *Nat. Phys.* **5** 647
[6] Wu D *et al* 2010 *Phys. Rev.* B **81** 100512
[7] Yang W L *et al* 2009 *Phys. Rev.* B **80** 014508
[8] Basov D N and Timusk T 2005 *Rev. Mod. Phys.* **77** 721
[9] Chu J-H *et al* 2009 *Phys. Rev.* B **79** 014506
[10] Wang X-F *et al* 2009 *Phys. Rev. Lett.* **102** 117005
[11] Wooten F 1972 *Optical Properties of Solids* (New York: Academic)
[12] Dressel M and Grüner G 2002 *Electrodynamics of Solids* (Cambridge: Cambridge University Press)
[13] Hu W Z *et al* 2008 *Phys. Rev. Lett.* **101** 257005

[14] Pfuner F *et al* 2009 *Eur. Phys. J.* B **67** 513
[15] Akrap A *et al* 2009 *Phys. Rev.* B **80** 180502
[16] van Heumen E *et al* 2009 arXiv:cond-mat/0912.0636
[17] Kim K W *et al* 2010 *Phys. Rev.* B **81** 214508
[18] Gorshunov B *et al* 2010 *Phys. Rev.* B **81** 060509
[19] Singh D J *et al* 2008 *Phys. Rev. Lett.* **100** 237003
[20] Yi M *et al* 2009 *Phys. Rev.* B **80** 024515
[21] Moon S J *et al* 2010 *Phys. Rev.* B **81** 205114
[22] Ashcroft N W and Mermin N D 1976 *Solid State Physics* (Philadelphia, PA: Holt-Saunders International Edition)
[23] Basov D N *et al* 1999 *Science* **283** 49
[24] Lester C *et al* 2009 *Phys. Rev.* B **80** 229901
[25] Benfatto L *et al* 2009 *Phys. Rev.* B **80** 214522
[26] Ortenzi L *et al* 2009 *Phys. Rev. Lett.* **103** 046404
[27] Nakajima M *et al* 2010 *Phys. Rev.* B **81** 104528